Biological Pattern Formation

Hardik Poptani

September 19, 2022

Contents

Summary

Chapter 1

Introduction

Chapter 2

Travelling Waves

The appearance of travelling waves appear in many biological phenomena such as in embryogenesis and in chemical reactions. It is known that in Keller's model as described in [2] was used to describe the concentration profile of the chemoattractant "aspartate" due to chemotaxis under presence of bacteria. Such appearance of these waves are a result of reaction-diffusion equations which are described below

$$\frac{\partial u}{\partial t} = D\frac{\partial^2 u}{\partial x^2} + f(u) \tag{2.1}$$

where for a concentration of a chemical $u(x,t)$ depending on space x and time t, we look at the change of concentration profile over time where D represents the constant diffusion coefficient and $f(u)$ is the function representing the "reaction" or kinetic terms of u. By solving for u, we find that the solutions of u are in the form of travelling waves, in which when graphically plotted, the shape of the wave remains the same as we can see a "shift". As travelling waves solution maintain a constant shape, we also say that the profile is "stable". In the absence of diffusion (when $D = 0$), we define the equilibria points as solutions u to equation 2.1 when

$$\frac{\partial u}{\partial t} = f(u) = 0 \tag{2.2}$$

where we can define the equilibria points as u_i from $f(u) = 0$ and the travelling waves will be stable in a region where $f'(u) < 0$.

In addition, since the solution is a travelling wave for all time, we see that the speed of this wave will be constant. We can define the speed as c along with introducing a change of coordinates ξ as:

$$\xi = x - ct, \quad u(x,t) = u(\xi) \tag{2.3}$$

since speed is constant thus making ξ constant. As ξ is constant, the shape of the travelling wave is constant thus u is also constant. Therefore, when we are finding

travelling wave solutions of an equation, we include the substitutions

$$\frac{\partial u}{\partial t} = -c\frac{du}{d\xi}, \quad \frac{\partial u}{\partial x} = \frac{du}{d\xi} \tag{2.4}$$

which therefore become ordinary differential equations in ξ. For reasons in biology, we must bound u for all ξ. Therefore, we can rewrite 2.1 as

$$0 = D\frac{d^2u}{d\xi^2} + c\frac{du}{d\xi} + f(u(\xi)) \tag{2.5}$$

and solve accordingly. We will look at a specific example of such an equation called the Fisher-Kolmogoroff Equation in the next section.

2.1 Fisher-Kolmogoroff Equation

The Fisher-Kolmogoroff Equation is a reaction-diffusion equation of the form of equation 2.1 as

$$\frac{\partial u}{\partial t} = D\frac{\partial^2 u}{\partial x^2} + ku(1-u) \tag{2.6}$$

where k and D are positive coefficients representing reaction and diffusion coefficients respectively, and $f(u) = ku(1-u)$. Since the coefficients k and D are constant, we can rewrite the system with a change of coordinates

$$\tilde{x} = x\left(\frac{k}{d}\right)^{1/2}, \quad \tilde{t} = kt \tag{2.7}$$

and removing the tilde for simplicity so that

$$\frac{\partial u}{\partial t} = \frac{\partial^2 u}{\partial x^2} + u(1-u) \tag{2.8}$$

along with $f(u)$ being defined respectively.

To check the equilibria points, we check for solutions u_i of $u(1-u) = 0$ in which we see that the solutions are $u_1 = 0$ and $u_2 = 1$. In addition, we see that $f'(u_1) > 0$ and $f'(u_2) < 1$, thus we should look for solutions where $0 \leq u \leq 1$.

For existence of travelling solutions, we can introduce the same variable from 2.3 where

$$\xi = x - ct, \quad u(x,t) = U(\xi) \tag{2.9}$$

where c is the speed defined earlier, and substituting to get the ordinary differential equation

$$U'' + cU' + U(1-U) = 0 \tag{2.10}$$

with respect to ξ. We note that the travelling "wavefront" solutions are such that as $z \to -\infty$, U is at one end of the steady state, and as $z \to \infty$, U is at the other end of the steady state. They are also known as the end boundary conditions for U for all ξ as required. Therefore, by solving the problem, we will find values of c to show the existence of the travelling wavefront solution.

From equation 2.10, we see that the $f(U)$ term is non-linear, therefore, we introduce another substitution variable $W(U)$ where

$$U' = W, \quad W' + cW + U(1-U) = 0 \tag{2.11}$$

and we check in the (U, W) phase plane. We found earlier that the equilibria points for u are 0 and 1 along with their stability respectively, thus we know that

$$\lim_{\xi \to -\infty} U(\xi) = 1, \quad \lim_{\xi \to \infty} U(\xi) = 0 \tag{2.12}$$

and the equilibria points are $(0, 0)$ and $(1, 0)$ respectively. We can rewrite fo W' as $W' = -cW - U(1-U)$, thus creating a matrix where

$$J = \begin{pmatrix} 0 & 1 \\ -1 + 2U & -c \end{pmatrix}$$

and by solving eigenvalues for J at each equilibria point, we see that

$$\lambda^{\pm}_{(0,0)} = \frac{-c \pm \sqrt{c^2 - 4}}{2}, \quad \lambda^{\pm}_{(1,0)} = \frac{-c \pm \sqrt{c^2 + 4}}{2} \tag{2.13}$$

The eigenvalues for $(1, 0)$ are both unstable as they show that $(1, 0)$ is a saddle point. However, we find that the eigenvalues of $(0, 0)$ both make it stable. If $c < 2$, then these eigenvalues make it a stable spiral point, and if $c > 2$, then the origin is a stable node point. To find the travelling wavefront solution, we omit $c < 2$ as the spiral would mean that $U < 0$ around the origin, which is unrealistic, thus for travelling wavefront to exist, $c > 2$ only. The graph is given from [1] as follows.

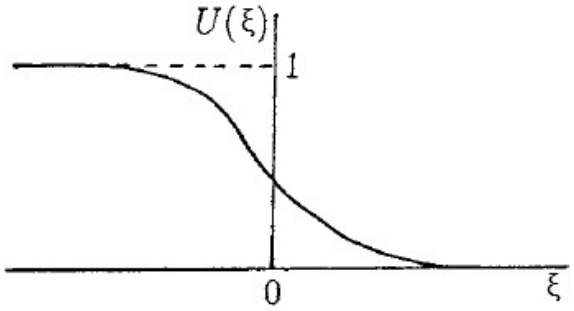

Figure 2.1: Travelling wavefront solution for the Fisher-Kolmogoroff equation where the speed $c > 2$. This figure is taken from [1].

2.2 Fitzhugh Nagumo Equations

In the previous section, we looked at a quadratic non-linear form for the reaction term. In this chapter, we will look at an example of a cubic from where

$$\frac{\partial u}{\partial t} = D\frac{\partial^2 u}{\partial x^2} + A(u-u_1)(u-u_2)(u-u_3) \tag{2.14}$$

where A is a positive reaction constant and $u_1 < u_2 < u_3$. To find travelling wavefront solutions, we must include

$$u(x,t) = U(\xi), \quad \xi = x - ct, \quad U'' + cU' + A(U-u_1)(U-u_2)(U-u_3) = 0 \tag{2.15}$$

and as it's non-linear,

$$U' = W, \quad W' = -cW - A(U-u_1)(U-u_2)(U-u_3) \tag{2.16}$$

where we find the equilibria points to be $(0,0)$, $(u_1,0)$, $(u_2,0)$, $(u_3,0)$. Along with finding the eigenvalues, we can determine the boundary conditions, ie

$$\lim_{\xi\to-\infty} U(\xi) = u_3, \quad \lim_{\xi\to\infty} U(\xi) = u_1 \tag{2.17}$$

We can then substitute to solve this by

$$DU'' + cU' + A(U-u_1)(U-u_2)(U-u_3) = 0 \tag{2.18}$$

As this is non-linear, we can make a substitution of $U' = \alpha(U-u_1)(U-u_3)$ where α is a constant and we included the equilibria points to rewrite the above equation as

$$(U-u_1)(U-u_3)[(2D\alpha^2 - A)U - [D\alpha^2(u_1+u_3) - c\alpha - Au_2]] = 0 \tag{2.19}$$

therefore to get non-trivial solutions, we must want

$$2D\alpha^2 - A = 0, \quad D\alpha^2(u_1+u_3) - c\alpha - Au_2 = 0 \tag{2.20}$$

which therefore we can determine α and the wavespeed c as

$$\alpha = \sqrt{\frac{A}{2D}}, \quad c = (u_1 - 2u_2 + u_3)\sqrt{\frac{AD}{2}} \tag{2.21}$$

Therefore, we can substitute back into the differential equation, and by integrating, we get the whole travelling wave solution

$$U(\xi) = \frac{u_3 + Ku_1 e^{\alpha(u_3-u_1)\xi}}{1 + Ke^{\alpha(u_3-u_1)\xi}} \tag{2.22}$$

where K is a positive constant.

As until now, we have been looking at equations in terms of one variable. However, in biological phenomena, there are multiple factors involved in such reaction-diffusion equations. In this section and later on in this dissertation, we will look at a system of two non-linear reaction-diffusion equations (including cubic terms) known as the Fitzhugh-Nagumo equation. In 1961 [3], Fitzhugh developed a model for wave propagation within the nerve membranes by using electrical impulses. The main task was to find out how it was made and how it works, thus mathematical models were based upon the cells within the nerve membranes also known as neurons. However the following year in 1962 [4], Nagumo proposed a model

$$\begin{aligned} \frac{\partial u}{\partial t} &= \frac{\partial^2 u}{\partial x^2} - k_u u(u-u_0)(u-u_1) - v \\ \frac{\partial v}{\partial t} &= D_v \frac{\partial^2 v}{\partial x^2} + e(u-v) \end{aligned} \tag{2.23}$$

which was an improvement of the previous model of [3] as Nagumo considered diffusion of the cells. In addition, it was assumed that there were no flux boundary conditions for both u and v. The variable u is considered to be an activator for the system while v is considered to be the inhibitor, meaning v accounts to decrease of production of u. In addition, D_v is the constant diffusion coefficient for v and k_u and e are the positive kinetic terms for u and v respectively.

To find the stability of the system, we must make

$$\begin{aligned} k_u u(u-u_0)(u-u_1) + v &= 0 \\ e(u-v) &= 0 \end{aligned} \tag{2.24}$$

where we find $u = v$, and we can substitute so that

$$u[k_u(u-u_0)(u-u_1)+1] = 0 \tag{2.25}$$

where we can immediately see that $(0,0)$ is a solution. The other two solutions would be of the form

$$u = \frac{u_0 + u_1 \pm \sqrt{u_0^2 + u_1^2 - 2u_0u_1 - 4/k_u}}{2} \tag{2.26}$$

For two real solutions to exist, we must make sure that the discriminant

$$u_0^2 + u_1^2 - 2u_0u_1 - 4/k_u > 0 \tag{2.27}$$

Since u_0 and u_1 are fixed, we can solve for k_u as we would find for 2 real solutions,

$$k_u > \frac{4}{(u_0-u_1)^2} \tag{2.28}$$

and similarly for a repeated real solution, $k_u = 4/(u_0 - u_1)^2$. In addition, we can check the stability of the equilibria points as well by checking the nullclines below.

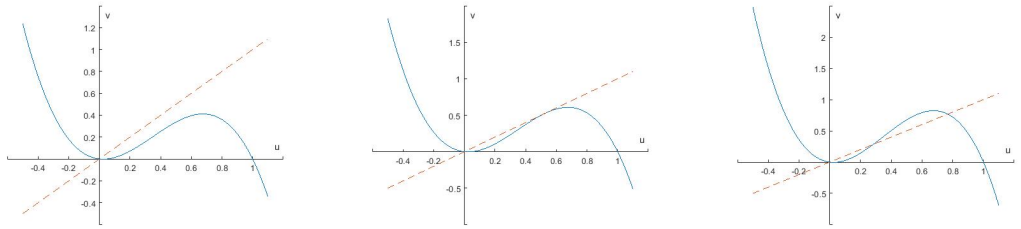

(a) One equilibrium point (b) Two equilibrium points (c) Three equilibrium points

Figure 2.2: Nullclines for equation 2.25 for each case. Blue line represents top line of 2.24 and red dashed line represents $v = u$. In all three figures, $u_0 = 0.05$ and $u_1 = 1$. Model parameters for $k_u = 3$ in 2.2a, $k_u = 4/0.95^2$ in 2.2b and $k_u = 6$ in 2.2c.

Since $k_u < 4/(u_0 - u_1)^2$ in 2.2a, there would be only one solution which is the origin. From the graph, we see that the origin is a stable point. Although the stability does allow travelling waves to appear, this means that both u and v concentrations will always be at 0, thus we will not be able to observe and change, and therefore there will be no travelling waves observed. For 2.2b, we now see that there is another solution apart from the origin. However, the second equilibria point is unstable, thus travelling waves cannot appear for this equilibria point, and we go back to the first condition in 2.2a. In figure 2.2c, we now see a total of three solutions representing the three equilibria points. The origin is stable, but will not produce travelling waves, and the second equilibria point is unstable. However, the third equilibria point is stable as well. Therefore, we can see a shift from the origin to the third equilibria point and vice versa as there will be areas of concentration at 0 and at another positive value. Therefore for travelling waves to appear, we must have the condition that $k_u > 4/(u_0 - u_1)^2$.

Going back to equation 2.23, there must be other conditions as well including the condition for diffusion. If the inhibitor diffusion is much smaller than the activator diffusion, we will get travelling waves, otherwise, we will get patterns which we talk more about in the next section. To check for travelling weave solutions, we shall solve for v as the inhibitor depends upon the solutions observed in the activator u profile. If travelling wave solutions are found for v, then we will also be able to observe travelling wave solutions in u. For simplification, we will replace the u profile as a rectangular profile by setting

$$u = \begin{cases} 1, & x \leq |a| \\ 0, & x > |a| \end{cases} \tag{2.29}$$

where a describes the boundaries of the medium. Other boundary conditions include $v(\infty) = v(-\infty) = 0$ assuming that v is continuously differentiable and $v(a) = v^+,\ v(-a) = v^-$ where v^+ and v^- represent the wavefront and back of the wave respectively. By using the substitution

$$\xi = x - ct, \quad D_v v'' + cv' + e(u - v) = 0 \tag{2.30}$$

and solving for each segment, we find that

$$v(\xi) = \begin{cases} v_1 e^{\lambda_2(\xi+a)}, & \xi < -a \\ 1 - \lambda_2 e^{\lambda_1(\xi+a)}/(\lambda_2 - \lambda_1) + \lambda_1 e^{\lambda_2(\xi-a)}/(\lambda_2 - \lambda_1), & -a \leq \xi \leq a \\ v_0 e^{\lambda_1(\xi-a)}, & \xi > a \end{cases} \tag{2.31}$$

where the eigenvalues are

$$\lambda_{1,2} = \frac{-c \pm \sqrt{c^2 + 4D_v e}}{2D_v} \tag{2.32}$$

We note that

$$v^+ = \frac{\lambda_2[1 - e^{2\lambda_1 a}]}{(\lambda_2 - \lambda_1)} \tag{2.33}$$

and

$$v^- = \frac{\lambda_1[e^{-2\lambda_2 a} - 1]}{(\lambda_2 - \lambda_1)} \tag{2.34}$$

To determine the existence of travelling waves, we can rewrite for v^- as $v^-(\lambda_2 - \lambda_1)/\lambda_1 + 1 = e^{-2\lambda_2 a}$. Since $0 < e^{-2\lambda_2 a} < 1$, we can see that $-1 < v^-(\lambda_2 - \lambda_1)/\lambda_1 < 0$, and thus replacing the eigenvalues to find that

$$D_v e < \frac{c^2 v^-(1 - v^-)}{(2v^- - 1)^2} \tag{2.35}$$

We note that the right hand side of the above inequality can be regarded as a constant, and thus we can rewrite this as

$$D_v < k/e \tag{2.36}$$

where $k = \frac{c^2 v^-(1-v^-)}{(2v^- - 1)^2}$. A graph of D_v against e^{-1} was shown in [5] where each region was specified

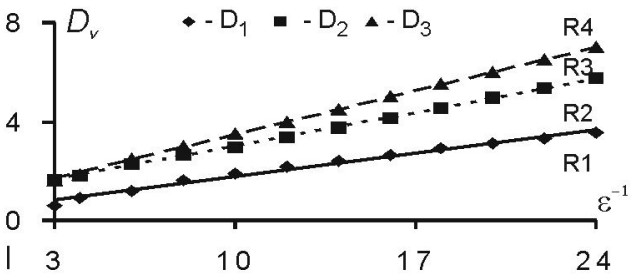

Figure 2.3: Parameter plane for domains corresponding to different dynamical regions as in [5]. For consideration of this dissertation, we have only looked at conditions for travelling wave noted in the region of $R1$ as from equation 2.36.

Now that we have the conditions, we can numerically integrate for the u profile as originally defined to see the travelling wave. The numerical integration was done on MATLAB and we can see from the 1D figures below

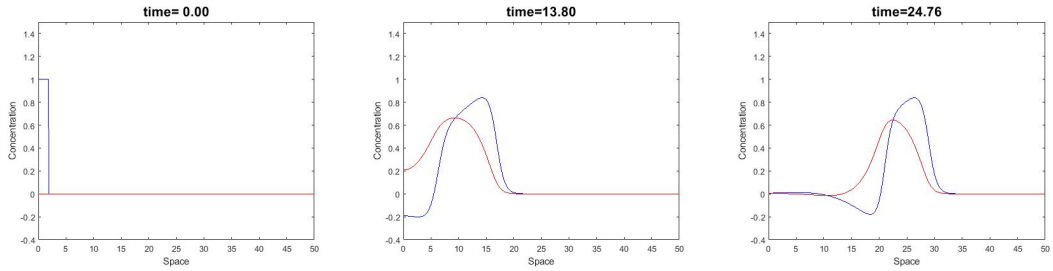

Figure 2.4: Travelling waves represented by the blue line for u and the red line for v. Time was taken for a total of 25 units. Model parameters are $D_v = 0$, $e = 0.3$, $k_u = 4.5$, $u_0 = 0.05$, $u_1 = 1$.

From the three figures above, we can see a gradual shift where we see the back and front of the wave. If continued for a longer period of time, we would see both of the waves completely disappear from the figure as the waves would keep on travelling in the forward direction. Initially, we see that the concentration of v is 0 everywhere meanwhile there is a small peak at 1 for the concentration of u and 0 everywhere else. We see that in the u profile, the peak at the front is around 0.9 and the trough is around -0.2. Meanwhile, the peak of v is around 0.6. We can see that the peak is the inhibitor is less than the peak of the activator. The purpose of the inhibitor is to slow down the production of the activator, thus we expect for v to have a smaller peak than u. We can also calculate that the speed of the travelling waves is 1.130.

As the main purpose of this dissertation is to see patterns, we will turn our attention to 2D space instead of 1D space. This is since we can easily spot patterns over 2D space. We now note that $u(\mathbf{x}, t)$ and $v(\mathbf{x}, t)$ where $\mathbf{x} \in \mathbb{R}^2$. We can replace x with $\mathbf{x}$ in equation 2.23, but since we are solving for travelling waves, we can use

the same substitution method as before for the 1D case. For the purposes of this dissertation, we have chosen the x space for substitution. This would also produce travelling waves. We can see the travelling waves for the u profile as shown below my numerical integration from MATLAB as seen below.

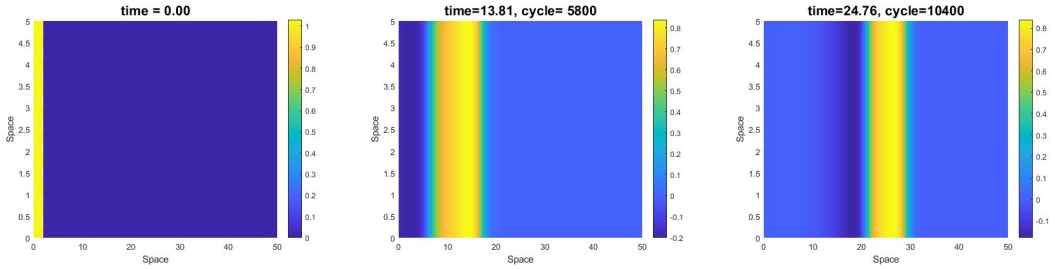

Figure 2.5: Travelling waves for u. Time was taken for a total of 25 units. Model parameters are $D_v = 0$, $e = 0.3$, $k_u = 4.5$, $u_0 = 0.05$, $u_1 = 1$.

This is very similar to what we've seen in figures 2.4. Initially, we can see the front of the wave as a peak, and thus as the time increases, we can see the wave shifting towards the right. The colourbar on the right is to show the intensity of the concentration levels for u. The peaks and troughs are as the same in the 1D case. The speed is calculated as previously. If we choose a line in the y axis, say $y = 3$, we will obtain the 1D case for u along this line.

As stated earlier in this section, the travelling waves observed from the FitzHugh-Nagumo model was used to conclude on how neurons travel within the nerve membrane via electrical impulses in [4]. Indeed, using a 2D scale can show multiple neurons moving along the line instead of the 1D scale. Since the electrical impulses were detected along the nerve membranes, it does make sense as to why we see a negative quantity of the trough of the travelling wave as it is known that current can flow in both directions. In the next section, we will talk about another type of pattern arising in the FitzHugh Nagumo model, and then we will combine the two to describe chemotaxis.

Chapter 3

Turing Patterns

In the previous chapter, we have talked about travelling waves and how they form spatial patterns as shown in figures 2.5. However, these are spatio-temporal patterns, meaning that these patterns formed from travelling waves can only be recognised over time, or even temporarily. Indeed, the time-varying position in space represented by ξ in the substitution of the previous chapter is an essential part of the entire pattern. In this chapter we will talk about the steady state ("static") spatially heterogeneous patterns also known as Turing Patterns. The name "Turing patterns" came from Alan Turing in 1952 [10] when he proposed conditions for such static spatio patterns. The conditions are the following for reaction-diffusion equations of the form

$$\begin{aligned} \frac{\partial u}{\partial t} &= D_u \frac{\partial^2 u}{\partial x^2} + f(u,v) \\ \frac{\partial v}{\partial t} &= D_v \frac{\partial^2 v}{\partial x^2} + g(u,v) \end{aligned} \tag{3.1}$$

as defined in the previous chapter:

1. In the absence of diffusion (net zero diffusion), two chemicals u and v would tend to go to an equilibrium state, thus being stable.
2. When there is a difference of diffusion between the two chemicals u and v, a small perturbation from equilibrium points will no longer make the system stay under equilibria, and thus the instability will lead to a change in spatial structure forming patterns.

We have already seen in the previous chapter how to find equilibria points, which is when $f(u,v) = g(u,v) = 0$. In addition, to find whether the points were stable or not for activator-inhibitor systems, we have only looked at graphical solutions. However, we can analyse the stability points by looking at the sign of $f'(u,v)$ and $g'(u,v)$ at u_0 and v_0 respectively. We want $f'(u_0,v_0)$ and $g'(u_0,v_0)$ to both be less

than 0. As f and g are functions of two variables u and v, we can write the Jacobian matrix as

$$M = \begin{pmatrix} f_u & f_v \\ g_u & g_v \end{pmatrix}_{(u_0,v_0)} \tag{3.2}$$

where each entry represents the first order differentiation of each variable at u_0 and v_0 respectively. In order to ensure stability, we must calculate the eigenvalues of the matrix and must make sure that the real entry of the eigenvalue is less than zero. In other words, we must make sure that

$$\begin{aligned} tr(M) &= f_u + g_v < 0 \\ det(M) &= f_u g_v - f_v g_u > 0 \end{aligned} \tag{3.3}$$

where $tr(M)$ and $det(M)$ represent the trace and determinant of the Jacobian M respectively. Thus we have found the conditions to satisfy the first point.

To satisfy the second point, we can represent a small perturbation of u and v by

$$\begin{aligned} \tilde{u} &= u - u_0 \\ \tilde{v} &= v - v_0 \end{aligned} \tag{3.4}$$

where $\tilde{u}$ and $\tilde{v}$ represent the changes, and u_0 and v_0 represent the equilibria points. By rearranging the top and bottom of equations 3.4, we can use taylor expansion for the first order for approximation as

$$f(u,v) = f(\tilde{u} + u_0, \tilde{v} + v_0) = f(u_0, v_0) + \tilde{u}\frac{\partial f(u_0,v_0)}{\partial u} + \tilde{v}\frac{\partial f(u_0,v_0)}{\partial v} \tag{3.5}$$

and similarly for $g(u,v)$. Higher order terms can be ignored as the perturbation terms are very small and can be approximated to 0. We can note that from equation 3.5, $f(u_0,v_0) = g(u_0,v_0) = 0$ as this is required from the first condition. Thus, we can substitute back into equation 3.1 and rewrite it as

$$\begin{aligned} \frac{\partial \tilde{u}}{\partial t} &= D_u \frac{\partial^2 \tilde{u}}{\partial x^2} + \tilde{u}\frac{\partial f(u_0,v_0)}{\partial u} + \tilde{v}\frac{\partial f(u_0,v_0)}{\partial v} \\ \frac{\partial \tilde{v}}{\partial t} &= D_v \frac{\partial^2 \tilde{v}}{\partial x^2} + \tilde{u}\frac{\partial g(u_0,v_0)}{\partial u} + \tilde{v}\frac{\partial g(u_0,v_0)}{\partial v} \end{aligned} \tag{3.6}$$

We can look for solutions for both equations of 3.6 by setting

$$\begin{aligned} \tilde{u}(x,t) &= we^{ikx+\lambda t} \\ \tilde{v}(x,t) &= qe^{ikx+\lambda t} \end{aligned} \tag{3.7}$$

where w and q are constants. Since we are looking for separable solutions, we can see that the x component is written as e^{ikx}. This means that we are looking for Fourier

mode solutions where k represents the wavenumber (Fourier number). Substituting this into equation 3.6, we get

$$\begin{aligned} \lambda w e^{ikx+\lambda t} &= -k^2 D_u w e^{ikx+\lambda t} + w e^{ikx+\lambda t} f_u + q e^{ikx+\lambda t} f_v \\ \lambda q e^{ikx+\lambda t} &= -k^2 D_v q e^{ikx+\lambda t} + w e^{ikx+\lambda t} g_u + q e^{ikx+\lambda t} g_v \end{aligned} \tag{3.8}$$

in which we can simplify to

$$\begin{aligned} 0 &= (-\lambda - k^2 D_u + f_u) w + f_v q \\ 0 &= (-\lambda - k^2 D_v + g_v) q + g_u w \end{aligned} \tag{3.9}$$

We can see from equation 3.9 that this is an eigenvalue problem. Let

$$b = \begin{pmatrix} w \\ q \end{pmatrix}, \quad D = \begin{pmatrix} D_u & 0 \\ 0 & D_v \end{pmatrix}$$

and M be defined as in 3.2 where we can substitute into 3.9 to get

$$0 = (M - k^2 D - \lambda \mathbf{I}) b \tag{3.10}$$

where $\mathbf{I}$ represents the 2×2 identity matrix. We can see that λ is the termporal growth rate and is an eigenvalue of the matrix $T = M - k^2 D$. Therefore, for instability, we must want either of one of the following conditions to hold

$$tr(T) = f_u + g_v - k^2(D_u + D_v) > 0 \tag{3.11}$$

$$det(T) = (f_u - k^2 D_u)(g_v - k^2 D_v) - f_v g_u < 0 \tag{3.12}$$

We know that $f_u + g_v < 0$ in the absence of diffusion. In addition, $D_u, D_v \in \mathbb{R}^+$, thus the trace $tr(T) < 0$ always. We can now look at the condition for the determinant of T. Expanding the determinant, we get

$$k^4 D_u D_v - (D_u g_v + D_v f_u) k^2 + (f_u g_v - f_v g_u) < 0 \tag{3.13}$$

We can see that this is a quadratic equation in terms of k^2. In addition, due to the first condition of formation of Turing patterns, we see that $f_u g_v - f_v g_u > 0$. Therefore, for this condition to hold, we must have $D_u g_v + D_v f_u > 0$. Moreover, looking at the discriminant, we must have

$$D_u g_v + D_v f_u > 2\sqrt{D_u D_v (f_u g_v - f_v g_u)} \tag{3.14}$$

so that k has one positive real part. In addition, if we impose zero flux boundary conditions where we define the boundaries of $x \in [0, L] \in \mathbb{R}$ where L is the length

of the boundary, we must restrict $k = n\pi/L$ where $n \in \mathbb{Z}$. Therefore, we can apply upper and lower bounds on k as $k_- < (n\pi/L)^2 < k_+$ where we can find $k_\pm$ by solving equation 3.13 using the quadratic formula. Therefore, by satisfying the second point from Turing, we are able to see a steady state with the absence of diffusion, but the system can become unstable when diffusion is present. We will see some examples of such activator-inhibitor systems and see how they can experience Turing patterns.

3.1 Gierer-Meinhardt Model

In 1972 [11], Gierer and Meinhardt proposed a reaction-diffusion equation model for activator-inhibitor systems. The objective was to show that their model can be used to show the formation of Turing patterns due to morphogenesis. As there are many modern day varients of the form, we will consider a simple version of this model

$$\begin{aligned} \frac{\partial u}{\partial t} &= D_u \frac{\partial^2 u}{\partial x^2} + \frac{u^2}{v} - bu \\ \frac{\partial v}{\partial t} &= D_v \frac{\partial^2 v}{\partial x^2} + u^2 - v \end{aligned} \tag{3.15}$$

where b is a constant regarding the degregation of the activator u. First, we must find the equilibria points of this equation. We can see that from the bottom bit of equation 3.15, $v = u^2$, and thus substituting back into the top bit, we see that $u_0 = 1/b$ and $v_0 = 1/b^2$ where u_0 and v_0 represent the equilibria points. To check that the equilibria points are stable, the Jacobian will be

$$R = \begin{pmatrix} b & -b^2 \\ 2/b & -1 \end{pmatrix} \tag{3.16}$$

which from the trace, we see that $b < 1$ and from determinant, $b > 0$, so for stability without diffusion, we note that $0 < b < 1$. Introducing the perturbation as defined in 3.5, we can rewrite equation 3.15 as

$$\begin{aligned} \frac{\partial \tilde{u}}{\partial t} &= D_u \frac{\partial^2 \tilde{u}}{\partial x^2} + b\tilde{u} - b^2\tilde{v} \\ \frac{\partial \tilde{v}}{\partial t} &= D_v \frac{\partial^2 \tilde{v}}{\partial x^2} + \frac{2}{b}\tilde{u} - \tilde{v} \end{aligned} \tag{3.17}$$

where we can denote solutions for $\tilde{u}$ and $\tilde{v}$ as in equation 3.7. Solving for eigenvalues, we can denote the new matrix

$$P = \begin{pmatrix} b - k^2 D_u & -b^2 \\ 2/b & -1 - k^2 D_v \end{pmatrix} \tag{3.18}$$

which by solving the determinant to determine instability, we get

$$k^4 D_u D_v - (bD_v - D_u)k^2 + b < 0 \tag{3.19}$$

thus we must have

$$bD_v - D_u > 2\sqrt{D_u D_v b} \tag{3.20}$$

In addition, if we want to see patterns, we must impose zero flux boundary conditions in a length of $x \in [0, L]$ at the end points. We will impose the condition that $k = n\pi/L$ as before where

$$\begin{aligned} k_-^2 &< \left(\frac{n\pi}{L}\right)^2 < k_+^2, \\ k_\pm &= \frac{(bD_v - D_u) \pm \sqrt{(bD_v - D_u)^2 - 4D_u D_v b}}{2D_u D_v} \end{aligned} \tag{3.21}$$

We observe another thing from this condition. We see that in order to have Turing Patterns, there must be a minimum and maximum length of the domain L. In addition, since n is an integer, we can see that if we increase the value of n, then the solutions would be periodic, meaning the patterns would repeat over a finite amount of length. Therefore, if we want to find the minimum critical length required (where $n = 1$), we find that

$$\frac{\pi}{k_+} < L \tag{3.22}$$

If we want to add an upper bound, the critical maximum length would be $L < \pi/k_-$. The upper and lower bounds applied in this case is when $n = 1$, which corresponds to the number of peaks and stripes as what we will see below. Therefore with these constraints, we can numerically integrate 3.1 on MATLAB and we can see the 1D figures below.

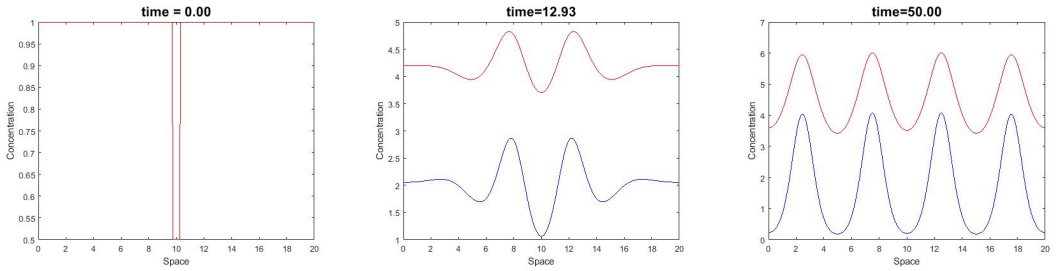

Figure 3.1: Turing patterns represented by blue line for u and red line for v. Time was taken for a total of 50 units. Model parameters are $D_v = 3$, $D_u = 0.1$, $b = 0.5$, $L = 20$.

From the three figures above, we see a change in pattern as the time increases. We notice that waves form at periodic intervals for both u and v, and then they become still at around the time at 36. The time was let to run till 50 to ensure that the waves formed will become still for the remaining time to ensure that the patterns have formed, and thus they will not deform. In addition, we see that the peaks and troughs for both u and v correspond at the same region in space. This is because u and v have solutions of forms of $le^{ikx+\lambda t} + z_0$ where l is a positive constant and z_0 would be the stability points for u and v respectively as mentioned in equations 3.5. However, the peaks and troughs for v are higher than u. This is due condition $bD_v - D_u > 0$. Since $0 < b < 1$ and both diffusion coefficients are positive, the inhibitor diffusion coefficient D_v is much larger than the activator diffusion coefficient D_u. Looking at the peaks, we see that there are a total of 4 peaks for u and v. Although we have mentioned that the critical length for patterns to form is $L > \frac{\pi}{k_+}$, if we add the upper bound at $n = 1$, that would correspond to L being much less than our model parameter for L. In fact, we could rewrite the top of equation 3.21 to get

$$\frac{Lk_-}{\pi} < n < \frac{Lk_+}{\pi} \tag{3.23}$$

From this condition and inputting the parameters, we find that $2.70 < n < 5.66$. As n is an integer, by rounding up on the lower bound and rounding down on the upper bound we see that $3 < n < 5$, which means $n = 4$. This means that n in our solution for the wavenumber k corresponds to the number of peaks seen. In fact, this shows that the solution formed is periodic as $n > 1$, thus we are able to see periodicity in figure **??**.

To illustrate it further, we can also represent Turing patterns of equations 3.15 in 2D. We will now let $u(\mathbf{x}, t)$ and $v(\mathbf{x}, t)$ where $\mathbf{x} \in \mathbb{R}^2$. We replace x with $\mathbf{x}$ in equations 3.15, and to solve, we now note that solutions will be of the form $e^{ik(x+y)+\lambda t}$ instead accounting $y \in \mathbb{R}$ for the extra dimension. In addition, we will alter our solutions for the wavenumber k and

$$k = \left(\frac{n\pi}{L_x}\right)^2 + \left(\frac{n\pi}{L_y}\right)^2 \tag{3.24}$$

where $L_x, L_y \in \mathbb{R}$ represent the lengths of the domain over the x and y plane. Therefore, to represent the bounds for $k_\pm$, we just represent the bounds for each axis as we have done for equation 3.21. To illustrate this in 2D, we can numerically integrate this in MATLAB and we can see the figures below.

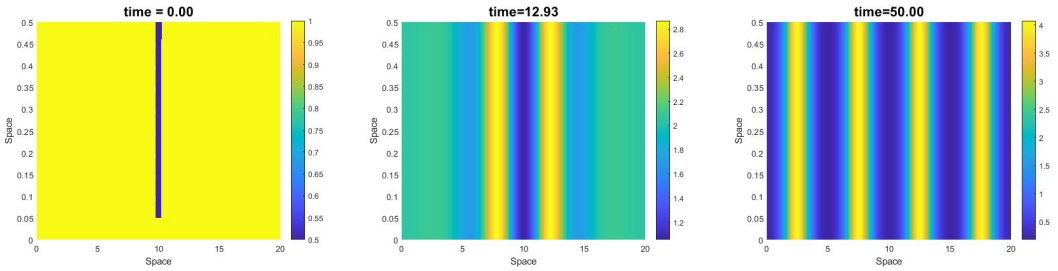

Figure 3.2: Turing patterns for u. Time was taken for a total of 50 units. Model parameters are $D_v = 3$, $D_u = 0.1$, $b = 0.5$, $L_x = 20$, $L_y = 0.5$.

From these three figures of figure 3.2, we see that this is very similar to the 1D version of u as seen in figures 3.1. Instead of peaks, we see stripes in the 2D version where the yellow stripes represent the "peaks" and the blue stripes represent the "troughs". In addition, we see exactly 4 yellow stripes. In fact, if we choose a y value from figure 3.2, we would get exactly the same pattern as we get in the 1D version of figures 3.1. We first see a small trough, and then we see that stripes eventually form, and this process stops at around a time of 36, but this was run to 50 so that we can notice that these stripes are now stationary, and they will not deform. In addition, the critical value for L in figures 3.1 to have stripes was $L > \pi/k_+$, which is approximately $L > 0.73$. In these figures, we have kept L_x as L before to be 20 and thus we see 4 stripes, however, our choice of $L_y < \pi/k_+$. Since this is the case, we would see no stationary patterns happen along the y domain. Therefore, the patterns appear as stripes in the x domain only.

However, if we change the condition for $L_y > \pi/k_+$, we would see patterns happening in both domains. We can numerically integrate this on MATLAB to see the phenomenon from the figures below.

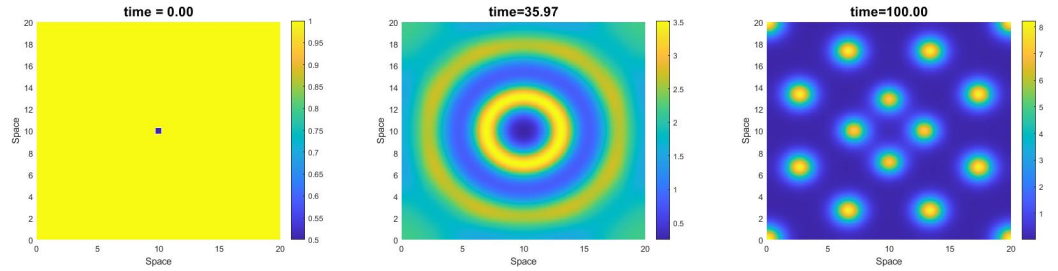

Figure 3.3: Turing patterns for u. Time was taken for a total of 100 units. Model parameters are $D_v = 3$, $D_u = 0.1$, $b = 0.5$, $L_x = 20$, $L_y = 20$.

In figure 3.3, we initially see a small dot which expands into concentric rings until around a time at 36. Afterwards, we start to see the concentric rings break down

into spots, starting with the far edge of the ring, and spots forming lastly on the closest ring to the centre. We note that the spots form along the yellow peaks of each concentric ring. This is since as the rings expand, the peaks acts as a propagating wave, but since the "peak" rings are unstable, at a critical time, the peak rings break down into stationary spots where the middle of the dot is the "peak". The farther the yellow ring is from the centre, the more unstable the ring is, thus the far-most ring broke down into spots much earlier at around a time of 36, meanwhile the inner bright yellow circle broke down into spots at around a time of 92. For a larger plane, we would see more formation of dots, and this might be the reason why we can see spots forming at the corners. In addition, since the radius of the inner yellow ring is much smaller than the outer ring, the size of the dots formed along the ring is much smaller, and the number of dots formed along the inner ring is much less. This is due to the fact that the spots do not have enough space to occupy. If we count the corners as well for the spots inside the domain, we see that there is a total of 16 spots which corresponds to 4x4 patterns forming at each domain. Since a value was chosen at 20 for the length of both domains, we would see a total of 4 peaks (or stripes) along the domain, thus in the 2D plane where we allow both domains to form patterns, we would see $4 \times 4 = 16$ stationary spots in total.

In fact, a result of this was used in a 1988 paper by JD Murray [13] to coat animal patterns in tails. He observed that leopards can either get stripes or spots at the tail during development. In fact, as the leopards grow over time, he noted that the stripes at the end of the tail would eventually change to stationary spots. In addition, such models of Turing Patterns can be used in other applications. We will now combine the result from this chapter and from the earlier chapter to show how Turing patterns can be formed in chemotaxis.

Chapter 4

Models of Chemotaxis

Chemotaxis is a chemo-mechanical process that is observed in many organisms. The process of chemotaxis is the movement of organisms in response to a chemical stimulus. This can range from many types such as in plants, bacteria, fungi, animals, and many more organisms. The process of chemotaxis is the movement of organisms in response to a chemical stimulus. For example, somatic cells in plants move according to areas of oxygen in the atmosphere, or in early development such as the migration of cells during embryogenesis. In this chapter,we will look at an example of how bacteria undergo chemotaxis. Bacteria undergo chemotaxis in order to get their food by detecting and moving towards a higher concentration of the food available. The detection is due to bacteria releasing a chemoattractant named "aspartate" which detects the concentrations of the food and causes bacteria to either move towards it or not. As bacteria undergo chemotaxis, we see that the movement of bacteria causes a shift within the aspartate. This is due to the fact that there might be more food as the bacteria approaches the attractant, thus the aspartate shifts towards the higher concentration of the food, however the aspartate's concentration doesn't decrease. In addition, the bacteria doesn't always keep on moving as some of the bacteria might die out or will become inactive during this process. As they have moved from their original position, they might end up in a situation where there is not enough food for them. This might cause an instability within the aspartate, which therefore leads to the bacteria being still at a region as the aspartate hasn't shifted.

In a paper from Berg [14], it was described how E-coli can undergo chemotaxis to form stable patterns of "surprising complexity but with remarkable regularity". Directly from experimenting with e-coli, the patterns cannot be described immediately, but mathematical models can be used to describe them. It was noted that their movement is random, and the diffusion coefficient was measured [9]. The experimental results carried by Berg showed that E-coli can form patterns when they feed on or are exposed to "tricarboxylic acid" when the bacteria are placed in a semi-solid substrate. The E-coli reacts to the chemical asparate, which leads to the patterns seen in figure [9] below.

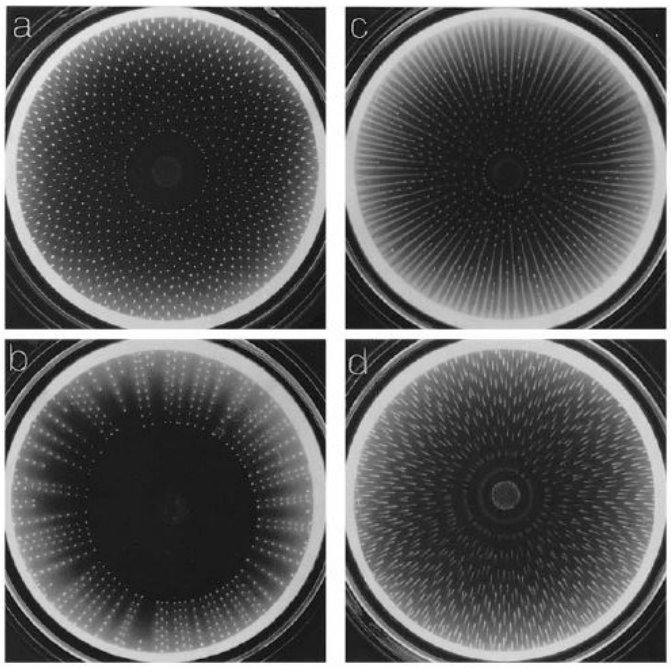

Figure 4.1: Adapted from [14], the E-coli was placed in semi-solid substrate of different concentrations in a petri dish. The light regions of asparate represent high density of bacteria. This figure is taken from [9].

Initially, the E-coli was inoculated at the centre of each petri dish. As the E-coli detect food inside the agar jelly, the aspartate is released inside the petri dish in the form of concentric rings, and the bacteria follow in the direction of the aspartate. The process keeps on happening until the E-coli reach the end of the petri dish, which afterwards, some of the aspartate breaks down into white spots as seen in figure 4.1. This is since the aspartate is now unstable as there is no more presence of the food left in the agar jelly. In all four figures of figure 4.1, we see that they all have a bright ring at the end of the petri dish as it would make sense since most of the bacteria have moved towards the end of the petri dish. Figure 4.1 a and d show that a sunflower pattern has been observed as most of the food was distributed evenly across the petri dish, hence the aspartate not being so unstable, and thus leaving the spots in form of the pattern across the petri dish. However, figure 4.1 c shows a radial streak pattern towards the edge of the petri dish since most of the food was towards the edges of the petri dish, and hence most of the aspartate were released in the following pattern.

From the conclusion of Berg [14], and from what we know about chemotaxis of bacteria, we can see that the concentric rings formed due to chemotaxis represents travelling waves, and after chemotaxis, we see that the spots formed inside the petri dish represent the stationary Turing patterns as what we have seen from chapters 2 and 3 of this dissertation respectively. We will be talking about this in more detail

using Keller-Segel's models for travelling waves [2] and in Turing patterns [12] to see how they are linked in chemotaxis.

4.1 Keller-Segel Model for Travelling Waves

In Keller's paper [2], a model was formulated to describe the bands (or areas) of active E coli. The bands of active E-coli are also representative to the areas of the aspartate released. These bands have been observed to travel at constant speeds when the bacteria experiences a chemotactic motion according to the chemoattractant. In other words, we can take the bacterial motion responding chemotactically to a single substrate, known as the "critical substrate". The model to describe such bands included partial differential equations which described the consumption of the critical substrate, ie the change in concentration, and the change in density due to random motion and chemotaxis. For conciseness, it was assumed that there was no growth of the E-coli, and the diffusion of the substrate denoted by D_c is a constant which is really small as compared to the "diffusive" motion of E-coli.

We denote c as the concentration of the substrate, and $\rho(x,t)$ as the bacterial density. It is assumed that the concentration $c(x,t)$ of space and time of the chemical is modelled by the equation

$$\frac{\partial c}{\partial t} = D_c \frac{\partial^2 c}{\partial x^2} - k_1 \rho \tag{4.1}$$

where k_1 is the constant rate of consumption of the substrate per cell, and D_c is the diffusion constant of the substrate.

The density of bacteria is modelled by the equation

$$\frac{\partial \rho}{\partial t} = \frac{\partial}{\partial x}\left(\mu \frac{\partial \rho}{\partial x}\right) - \frac{\partial}{\partial x}\left(\rho \chi \frac{\partial c}{\partial x}\right) \tag{4.2}$$

where μ parameter takes place of the diffusion coefficient, and χ is the chemotactic coefficient. In Keller's paper [2], both of the coefficients are as a function of the concentration c. The term $\frac{\partial}{\partial x}(\mu \frac{\partial \rho}{\partial x})$ represents the motion of bacteria albeit chemotaxis. If there is no chemical gradient, ie $\frac{\partial c}{\partial x} = 0$, the equation becomes identical to the diffusion equation. The random motion of bacteria unaffected by chemotaxis suggests that the flux of E-coli is proportional to the gradient in density.

In a previous study by Alder and Dahl [15], the random motion of E-coli is "similar to diffusion" where there was no chemical gradient. This motion was detected by μ and was taken to be a constant. Alder and Dahl [15] looked for solutions to equations 4.1 and 4.2 to the first approximation such that D_c equals zero.

The term $\frac{\partial}{\partial x}(\rho \chi \frac{\partial c}{\partial x})$ represents the response of the bacteria due to chemotaxis. Since it is assumed that the flux is proportional to the chemical gradient, it was

shown that the chemotactic response was insufficient for weak gradients. The flux due to chemotaxis was denoted as $\rho\chi\frac{\partial c}{\partial x}$ where χ is the measure of strength of the chemotaxis, thus the "chemotactic coefficient".

Under the assumptions made so far, $\chi(c)$ must have been singular for equations 4.1 and 4.2 to produce travelling bands as a solution. Thus it was assumed that the chemotactic coefficient was represented as

$$\chi(c) = \delta c^{-1} \tag{4.3}$$

where δ is a constant.

Solutions of equations 4.1 and 4.2 were found in Keller's paper [2], and the derivations were solved in [16]. Since these are partial differential equations, the initial boundary conditions were chosen such that

$$c(x,0) = c_\infty, \quad \rho(x,0) = \rho_\infty \tag{4.4}$$

where these are both constants. Assuming that $x \in [0, L]$ where L is the maximum length of the tube and the bacteria did not flow at the endpoints,

$$\frac{\partial c}{\partial x} = 0, \text{ and } \frac{\partial \rho}{\partial x} = 0 \text{ at } x = 0 \text{ and } x = L \tag{4.5}$$

Since the solutions in the form of a band are the "travelling waves", it was allowed to take an infinite length of the tube, ie let x vary from $-\infty$ to ∞, and look for solutions of the form

$$\rho(x,t) = \rho(\bar{\xi}), \quad c(x,t) = c(\bar{\xi})$$

where a change of coordinates

$$\bar{\xi} = \frac{s}{\mu}(x - st) \tag{4.6}$$

has been introduced, and s is the constant speed band. Also, the boundary conditions imply that

$$\rho \to 0, \quad \rho' \to 0, \quad c \to c_\infty, \text{ as } \xi \to \infty \tag{4.7}$$

Therefore, we solve for $c(\bar{\xi})$ and $\rho(\bar{\xi})$ as

$$c(\bar{\xi}) = c_\infty(1 + e^{-\bar{\xi}})^{1/(1-\bar{\delta})} \tag{4.8}$$

$$\rho(\bar{\xi}) = \frac{s^2 c_\infty e^{-\bar{\xi}}(1 + e^{-\bar{\xi}})^{\bar{\delta}/(1-\bar{\delta})}}{\mu k_1(\bar{\delta} - 1)} \tag{4.9}$$

As $\bar{\xi} \to -\infty$, ρ and c behave as multiples of $e^{\bar{\xi}/(\bar{\delta}-1)}$. Assuming that solutions were finite, this implies that $\bar{\delta} > 1$ or $\delta > \mu$, and thus

$$\lim_{\bar{\xi}\to-\infty} c = 0, \quad \lim_{\bar{\xi}\to-\infty} \rho = 0 \tag{4.10}$$

Integrating ρ and taking limits, it was obtained that the speed of the traveling bands can be denoted as

$$s = \frac{Nk_1}{ac_\infty} \tag{4.11}$$

where N is the total number of bacteria found in the band and a is the cross-sectional area of the tube used in the experiment.

Graphs of equations 4.8 and 4.9 for c and ρ against $\bar{\xi}$ were given in MATLAB figures as below.

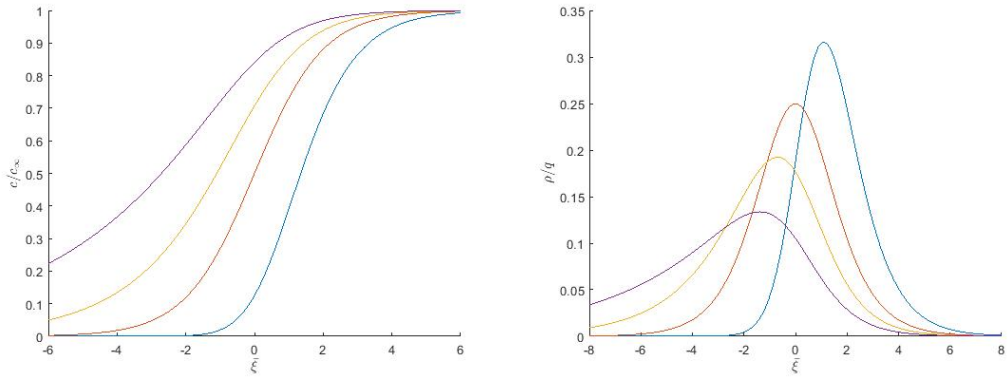

Figure 4.2: Graphs for critical substrate concentration c and density of bacteria ρ against $\bar{\xi}$ where model parameters are $\mu = 1/4$, $k_1 = 5$ x 10^{-12}, and $c_\infty = 2$ x 10^{-4}, $\bar{\delta} = 2$, $\bar{\delta} = 3$, and $\bar{\delta} = 5$.

A higher value of $\bar{\delta}$ corresponds to a higher chemotaxis strength δ as it was assumed that the diffusion coefficient μ remained constant for each chemical. As they all exhibit travelling solutions, for a higher value of $\bar{\delta}$, the concentration is higher at the left side of the graph, and then the shift becomes shallower and the value is less on the right side of the graph. This may be due to the fact that for a stronger chemotactic agent, the E-coli gets attracted to the chemical and eats the chemical faster resulting in a higher value on the left, and later on, the abundance of the chemical have decreased more than the ones with weaker chemotactic strength, so this results in a shallower gradient at the right side of the graph. Therefore, the travelling waves for a higher value of $\bar{\delta}$ will not move as mush to the equilibrium state as for ones with lower values of $\bar{\delta}$. All values of $\bar{\delta}$ tend to an upper limit denoting that the chemical may have been fully consumed.

Note that around $\bar{\delta} = 2$, the curve is symmetrical, and is steeper at the right side when $\bar{\delta} > 2$, and at the left side when $\bar{\delta} < 2$. For low values of $\bar{\delta}$, the width is very narrow, and wider for larger values. We can tell that for a stronger chemotactic agent, the diffusion of the chemical will be minimal, thus for a stronger chemotactic

agent, the bacteria will move more rapidly, and thus will be able to spread uniformly which coincides with the larger width. This can correspond to figure 3.1 where for a higher strength of chemotaxis, the bacteria are spread out more, thus there will not be a major shift for the travelling waves of the chemical.

The results produced in the paper was nearly exact to the results obtained in Alder and Dahl's paper [15] for modelling E-coli. From the results, it was decided that this model was capable of describing both chemotactic bands of moving bacteria and the aggregation of slime mould in another paper, and thus this model can be extended to other chemotactic phenomena.

We have look at the travelling wave solutions, and now we will extend this to when the stationary spots being formed in the next section.

4.2 Pattern Formation on Keller-Segel Model

In the previous section, we assumed that there was neither no growth or death rate of bacteria, nor the production rate of the substrate. We will modify equations 4.2 and 4.1 to the following:

$$\frac{\partial \rho}{\partial t} = \mu \frac{\partial \rho^2}{\partial x^2} - \kappa \frac{\partial}{\partial x}\left(\frac{\rho}{(1+c)^2}\frac{\partial c}{\partial x}\right) + a\rho(1-\rho) \tag{4.12}$$

where a is considered to be the growth (or death) rate of bacteria for the density equation 4.12. In addition, we now assume that the chemotactic strength κ is a constant, and the chemotaxis term also depends on c^{-2}. In addition, we will write the change for the concentration density as

$$\frac{\partial c}{\partial t} = \frac{\partial^2 c}{\partial x^2} + \frac{\rho^2}{1+\rho^2} - \rho c \tag{4.13}$$

In Alder's paper [15], along with the cell density and concentration of the substrate, the concentration of the nutrient (food) was considered to make the patterns. However, since the consumption of the nutrient was very small, for the purposes of this dissertation, we will ignore the change in concentration of the nutrient. As we are wanting to find stationary solutions, we must first find the equilibria points. In equation 4.12, we note that there is a chemotaxis term along with a diffusion term. Since chemotaxis term is also considered to be part of the flux, at equilibria, it is assumed that there is no chemotaxis happening, thus we assume that $\kappa = 0$ at equilibria. Therefore to find the equilibria points, we make

$$\begin{aligned} \frac{\partial \rho}{\partial t} &= a\rho(1-\rho) = 0 \\ \frac{\partial c}{\partial t} &= \frac{\rho^2}{1+\rho^2} - \rho c = 0 \end{aligned} \tag{4.14}$$

in which we find that $\rho = 0$ or $\rho = 1$. If $\rho = 0$, then we could allow any value of c, however, wee will choose $\rho = 1$ such that $c = 1/2$. To check the stability, we make the Jacobian

$$R = \begin{pmatrix} -2a\rho + a & 0 \\ \frac{2\rho}{(1+\rho^2)^2} & -\rho \end{pmatrix} \tag{4.15}$$

and when substituting $\rho = 1$, we find that $tr(R) = -a - 1 < 0$ thus $a > -1$, and $det(R) = a > 0$, therefore the only condition required is $a > 0$. Introducing a small perturbation as defined in 3.5, we get

$$\begin{aligned} \frac{\partial \rho}{\partial t} &= \mu \frac{\partial \rho^2}{\partial x^2} - \frac{4}{9}\kappa \frac{\partial^2 c}{\partial x^2} - a\rho \\ \frac{\partial c}{\partial t} &= \frac{\partial^2 c}{\partial x^2} + \frac{\rho}{2} - c \end{aligned} \tag{4.16}$$

where we can denote solutions for ρ and c as in equation 3.7. Solving for eigenvalues, we can denote the new matrix

$$P = \begin{pmatrix} -a - k^2\mu & \kappa(4/9)k^2 \\ 1/2 & -1 - k^2 \end{pmatrix} \tag{4.17}$$

which by solving the determinant to determine instability, we get

$$\mu k^4 - (-\mu - a + \frac{2}{18}\kappa)k^2 + a = 0 \tag{4.18}$$

thus we must have

$$-\mu - a + \frac{2}{18}\kappa > 2\sqrt{\mu a} \tag{4.19}$$

In addition, if we want to see patterns, we must impose zero flux boundary conditions in a length of $x \in [0, L]$ at the end points. We will impose the condition that $k = n\pi/L$ as before where

$$\begin{aligned} &k_-^2 < \left(\frac{n\pi}{L}\right)^2 < k_+^2, \\ &k_\pm = \frac{(-\mu - a + 2\kappa/18) \pm \sqrt{(-\mu - a + 2\kappa/18)^2 - 4\mu a}}{2\mu a} \end{aligned} \tag{4.20}$$

Thus the critical length required would me $L > \pi/k_+$. Therefore, we can numerically integrate in MATLAB to produce the figures for equations 4.12 and 4.13 below.

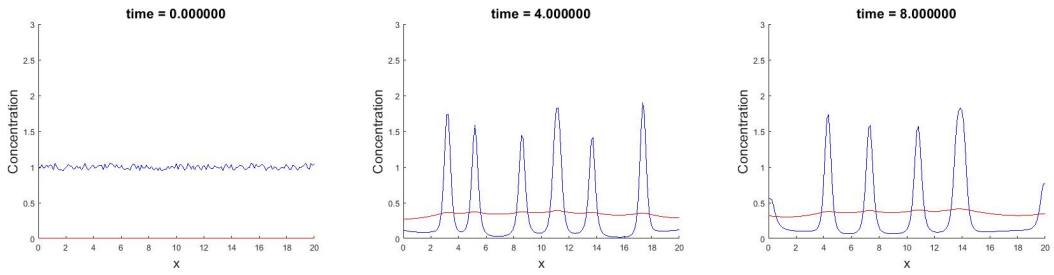

Figure 4.3: Patterns observed for ρ in blue and c in red. Model parameters are $\mu = 0.25$, $a = 1$, $\kappa = 90$, $L = 20$.

Initially, we set a small perturbation for ρ by adding noise in the MATLAB code, and set $c = 0$. Due to the random distribution, we see many peaks and troughs for ρ. This might be due to the fact that the bacteria have started to release the chemoattractant. This corresponds with the sudden increase of c. As time increases, the bacteria continue to release the chemoattractant. However, we note that the concentration of the chemo attractant is not changing as much over time. This may be to to the fact that when some of the food are no longer present, the chemoattractant dissolves in the nutrient jelly, therefore, we see little to no net change in c. Meanwhile, as time increases, we see that the number of peaks decreases, but the amplitudes increases. This may be due to the fact that there might be competition going on within the bacterial species. The denser the group of cells, the greater the production of chemoattractant. However, the high cell density group of cells also experience diffusion much more against them, which also may be a reason why there is no net change in c. If not enough chemoattractant is produced to overpower diffusion, then the group with higher chemoatttractant production rate than diffusion rate would not die out as fast, even if they are in lower numbers. Therefore, we see a reduction in the population of high density corresponding to less peaks. Eventually, the patterns of high cell concentrations start to disappear, however, there will be some (or maybe one) peak left over. The left over peak would be the stable peak and possibly some left over bacteria.

Chapter 5

Conclusion

In this dissertation, we introduced the notion of pattern formation and its applications to biology. Such examples were the waves produced of calcium concentration during embryo development. The waves formed from the calcium signals are known as travelling waves, and we have first analysed them on how they appear and their conditions required for such waves to appear. In addition, we have also given examples such as spots formed on giraffes or stripes formed on snakes, or even on nonliving objects such as the shell of molluscs. These patterns are known to be permanent on them, and unlike the travelling waves, these patterns are known to be stationary in which they are commonly known as "Turing Patterns". Patterns like these arise during morphogenesis, which is the early stage of life that involve reaction-diffusion equations. In addition, such patterns can also arise in other biological phenomena such as chemotaxis. In the last chapter, we combined the studies from travelling wave solutions and stationary patterns to see how they arise in chemotactically moving bacteria.

In the first chapter, we explicitly discussed travelling wave solutions, first from the Fisher-Kologroff equation, and then from the Fitzhugh Nagumo (FHN) model. Assuming that there was no flux boundary conditions, we analysed the conditions for such propagation of the wave to happen for the Fisher-Kologroff equation, and then we saw a graph of such travelling waves. The Fisher-Kologroff equation was a term of quadratic in the concentration, meanwhile the FHN model was more interesting as it included a cubic term, and the FHN model involed two chemical interactions instead of a solo interaction. In addition, the FHN model was used to describe electrical impulses from neurons and how they propagate. We then analysed the conditions for travelling wave solutions for the FHN model, and have used numerical methods on MATLAB to numerically integrate the FHN equations, and to see the animation for the 1D and 2D models respectively. The major advantage of numerical methods is that we can see the propagation of waves over a specific time period. In addition, the error from the numerical methods is very small since the numerical methods were forms of difference equations, which tie in neatly with the partial differential equations. Nevertheless, the 2D model gave a greater understanding of the travelling

wave in space rather than over a single domain as in the 1D version.

In the second chapter, we now looked at stationary (static) patterns. Unlike travelling wave solutions, these stationary solutions are formed due to a small perturbation of instability. These patterns were first theorised by Alan Turing, and thus commonly known as Turing Patterns. We first discussed the conditions of such static patterns arising, and then we gave an example of such on the Gierer-Meinhardt (GM) model. The objective of this model was to show that the model can be used for the formation of Turing Patterns due to morphogenesis. We have analysed the conditions for Turing Patterns to form on the GM model, and then have used MATLAB to numerically integrate the GM equations for 1D and 2D respectively. In the 1D version, we have seen the peaks and troughs of waves that eventually become stable. To see the patterns more explicitly, we turned attention to the 2D model where we have seen two different types of patterns: stationary spots and stripes. We note that these patterns are due to the different lengths of the medium. For a medium below the critical length, we see stipes, otherwise we would see spots. Indeed, if we changed the inital conditions of our spot formation pattern in 2D so that we are integrating over one domain only, we would see stripes as well. Like in the previous chapter, we have considered numerical methods which were accurate as they were also in the form of difference equations tying in with the partial differential equations.

Finally, we have linked the two types of patterns observed in the previous chapters to see how such patterns arise in chemotaxis instead of morphogenesis. The major difference is that now the chemotaxis term is also included for flux. In this chapter, we have used versions of Keller-Segel models to illustrate travelling waves of E-coli and patterns of E-coli. By analysing travelling wave solutions, we first derived the solutions for the concentration of the chemoattractant and density for the E-coli, in which we plotted the graphs of the functions for each describing them. Although they were linked together, we were not able to see how the two evolve over time. If time permitted, we would've used a different method of integration instead of the standard method used for the previous two chapters. The difficulty arose from the fact that the chemotaxis term included a c^{-1} term, thus the difficulty was to avoid the code blowing up due to the singularity at around $c = 0$. Afterwards, we modified the Keller-Segel equations by also involving proliferation of the E-coli and the production of the concentration of the chemoattractant along with the degradation. The kinetic terms were added so that we could be able to analyse the stability around a non-zero point, which would allow us to introduce a small perturbation. After analysing the conditions, we numerically integrated to plot the graphs of them by using the Lax-Friedrichs method. This method was used to overcome the singularity arising due to the c^{-2} term, in which this code can be seen in the appendix. Overall, we have seen how travelling wave and stationary spot patterns have been used to tie in with Alder's paper [15] and how they can be used to study chemotaxis. Further studies can be done to explore such patterns that can be seen due to chemotaxis on other models as well.

Bibliography

[1] J. D. Murray; Mathematical Biology: I. An Introduction; pages 438-439; Springer; Third Edition; 2002

[2] Evelyn F. Keller And Lee A. Segel; Traveling Bands of Chemotactic Bacteria: A Theoretical Analysis; pages 235-248; Journal of Theoretical Biology; 30; 1971

[3] Richard Fitzhugh; Impulses And Physiological States In Theoretical Models Of Nerve Membrane; Biophysical Journal; Volume 1; 1961

[4] J. Nagumo, S. Arimoto, and S. Yoshizawa; An Active Pulse Transmission Line Simulating Nerve Axon; pages 2061-2070; Proceedings of the Ire; 1962

[5] B. Vasiev; Classification of patterns in excitable systems with lateral inhibition; Phys Lett. A.; 323; 194-203; 2004

[6] O. Vasieva, M. Rasolonjanahary and B. Vasiev; Mathematical modelling in developmental biology; Reproduction (Cambridge, England); 145; R175-84; 2013

[7] B.Vasiev, A. Panfilov, R. Khramov; Large pulsating waves in a one-dimensional excitable medium; Physics Letters A; 192; 227-232; 1994

[8] Manan'Iarvo Louis Rasolonjanahary; Scaling of morphogenetic patterns in continuous and discrete models; PHD Thesis; University of Liverpool; 2013

[9] J. D. Murray; Mathematical Biology II: Spatial Models and Biomedical Applications; pages 71-90; Springer; Third Edition; 2003

[10] A. M. Turing; The Chemical Basis of Morphogenesis; Philosophical Transactions of the Royal Society of London; Series B; Biological Sciences; 237; pages 37-72; 1952

[11] A. Gierer and H. Meinhardt; A Theory of Biological Pattern Formation; Max-Planck-Institut ftir Virusforschung, Ttibingen, Germany; Kybernetik; Springer-Verlag; 12; pages 30-39; 1972

[12] Evelyn F. Keller and Lee A. Segel; Initiation of Slime Mold Aggregation Viewed as an Instability; pages 399-415; Journal of Theoretical Biology; 26; 1970

[13] Murray, J. D.; How the leopard gets its spots; Scientific American; 258; 3; 80–87; 1988

[14] Elena O. Budrene and Howard C. Berg; Dynamics of formation of symmetrical patterns by chemotactic bacteria; pages 49-50; Letters to Nature; 1995

[15] Adler J. and Dahl, MM; A Method For Measuring Motility Of Bacteria And For Comparing Random And Non-random Motility; Journal of General Microbiology; 46; 1967

[16] Hardik Poptani; Modelling chemotactic motion of cells; Master's preliminary dissertation; University of Liverpool; 2022

[17] Rebecca C. Tyson; Pattern Formation by E-coli - Mathematical and Numerical Investigation of a Biological Phenomenon; PHD Thesis; University of Washington; 1996